# The Passivating Layer Influence on Mg-based Anode Corrosion and Implications for Electrochemical Struvite Precipitation

*László Kékedy-Nagy*[a], *John P. Moore II*[a], *Mojtaba Abolhassani*[a], *Faridreza Attarzadeh*[a,†], *Jamie A. Hestekin*[a], *and Lauren F. Greenlee*[a]*

[a] Ralph E. Martin Department of Chemical Engineering, University of Arkansas, 3202 Bell Engineering Center, Fayetteville, Arkansas 72701, United States

[†]Current affiliation: Department of Mechanical Engineering, The University of Memphis, 312 Engineering Science Bldg, Memphis, Tennessee 38152, United States

Corresponding author: Tel.: 610-507-6390, E-mail: greenlee@uark.edu

**Abstract.**

The removal and recycling of phosphorous from wastewater streams by electrochemical precipitation of struvite is a new and exciting approach; however, previous studies showed low percent yields in single cell batch experiments without pH adjustment. To investigate improvement of the percent yield, the surface-area-to-volume ratio of the electrodes was increased by 1.9-fold; consequently, a 27% increase in struvite production was observed for the pure-Mg anodes, but only a 2% increase for the AZ31 alloy. Potentiodynamic polarization experiments revealed 1.8-fold higher corrosion rates for the AZ31 alloy, which is in contradiction with the 2.8-fold higher magnesium dissolution rates calculated for the pure-Mg during struvite precipitation. This discrepancy between the techniques is attributed to the difference in the electrochemical environment, where the formation of an insulating layer of struvite on the anodes during the batch precipitation experiments is a critical difference. Based on characterization of the morphology and chemical structure of the precipitate, studied by Fourier-transform infrared spectrometry and scanning electron microscopy, pure struvite was obtained with a particle size of ca. 73 µm in length and ca. 13 µm in width for pure-Mg and ca. 44 µm in length and ca. 8 µm in width for the AZ31 alloy anode, respectively.

## Introduction

The removal of excessive nutrients like nitrogen and phosphorus from wastewater streams has become essential to avoid water quality degradation or eutrophication of the receiving waterbodies and to meet the legal requirements enforced on wastewater disposal.[1, 2] One simple way to remove these nutrients is by precipitation as magnesium ammonium phosphate hexahydrate ($MgNH_4PO_4*6H_2O$), also known as struvite, a poorly soluble mineral with an orthorhombic crystal structure.[3, 4] Struvite is well-known to wastewater plant operators because the mineral causes blockages in pipes and pumps, therefore increasing operating costs.[5, 6] On the other hand, struvite is also considered to be a slow-releasing, premium-grade fertilizer and can be used successfully in agriculture.[7, 8]

Struvite crystallization depends on factors such as the ratios of $Mg^{2+}$, $NH_4^+$, and $PO_4^{3-}$ ions, ionic strength, potentially interfering ions (especially divalent cations), and pH, where the latter is generally considered to be a key factor.[9, 10] Chemical precipitation of struvite is a widely used technique. However, a drawback of chemical precipitation is the required addition of extra chemicals (i.e., magnesium salt and base) into the water. On the other hand, electrochemical precipitation of struvite in wastewaters is a new approach where a sacrificial magnesium-based anode is used as the only source for magnesium and hydroxyl anions are generated, eliminating the addition of extra chemicals.[11, 12] The electrochemical reactions involved in the struvite precipitation were described in detail by others,[9, 11, 13-15] and the overall reaction can be described as:

$$Mg^{2+} + NH_4^+ + H_nPO_4^{n-3} + 6H_2O \rightarrow MgNH_4PO_4 * 6H_2O \downarrow + nH^+ \quad (1)$$

where n = 0, 1 or 2 is based on the solution pH.[16, 17] The electrochemical precipitation of struvite is strongly dependent on the corrosion rate of the magnesium-based anode. Nonetheless, the formation of a passivating layer of struvite, reported by others and observed in our previous experiments,[13-15, 18] on the surface of the anode during the electrochemical precipitation complicates the overall process by having a negative effect on the struvite production.

The corrosion behavior of pure-Mg and Mg-alloys has been studied previously[19-23] and was shown to significantly depend on the medium to which the magnesium material is exposed.[24] These corrosion studies performed on pure-Mg and Mg-alloys have revealed that accurate corrosion rates are difficult to obtain, and there are certain inconsistencies between the corrosion rates obtained by

electrochemical and gravimetric methods. The corrosion rates obtained by the electrochemical approach were shown to produce an underestimation of the Mg corrosion compared to the ones obtained by weight loss measurements.[25-27] This discrepancy was associated with various causes, e.g., material disintegration,[28] anomalous chemical dissolution[29] (NB: This can coincide with electrochemical corrosion), or with limitations in the application of the Stern-Geary equation.[30] For this reason, the corrosion rates obtained in this work by electrochemical methods should be considered as relative values rather than absolute, where they are presented as a comparison between the pure-Mg and the AZ31 Mg alloy.

The objectives of this work were to improve the percent yield of electrochemical struvite precipitation in an acidic environment without pH adjustment by increasing the surface-area-to-volume ratio (SV/A) and to study the effect of the insulating layer formed during batch experiments on the corrosion rate of the magnesium-based sacrificial anode (see Figure 1). The morphology and the composition of the electrochemically precipitated struvite were investigated by Fourier-transform infrared spectrometry (FT-IR), x-ray diffraction (XRD) and scanning electron microscopy (SEM).

**// Figure 1 //**

## Experimental

### 2.1. Materials

The ammonium dihydrogen phosphate ($NH_4H_2PO_4$) was purchased from Sigma-Aldrich, and the test solutions were prepared by using Milli-Q water (18.2 MΩ, Millipore, Bedford, MA, USA). The pH of the bulk test solution was measured before and after the experiments by using a digital pH meter (Orion Star A111, Thermo Scientific). The high purity Mg (99.9% pure), AZ31 Mg alloy (Al 3 *wt*%, Zn 1 *wt*%, balance Mg) and stainless-steel (316SS) plates (5 x 5 cm; 2 mm thick) were purchased from Goodfellow Corporation. The plates were cleaned by mechanical polishing, using sandpaper with different grain sizes, purchased at a local hardware store.

### 2.2. Reactor setup and electrolysis experiments

The batch struvite precipitation experiments were conducted in a single-compartment reactor as described in our previous studies, with small modifications. The reactor was filled with approx. 450 mL of the test solution (0.077 M) and was continuously stirred at ~220 rpm. The batch experiments lasted for 6 h at a fixed anode potential of -0.8 V, proposed previously by others,[14] controlled with a VSP-300 multichannel potentiostat/galvanostat (Bio-Logic, USA) and measured against a double-junction Ag/AgCl (3M NaCl, BASi) reference electrode. The graphic illustration of the experimental setup is shown in Figure. 1, where pure-Mg or the AZ31 alloy served as the anode, and 316SS served as the cathode. The 25 $cm^2$ size plates with an active surface area of ~40 $cm^2$ (both sides of the electrodes were used) were placed at a distance of 5 cm from each other. The precipitates formed on the anode and cathode were collected by scraping the electrode carefully with a razor, while the precipitate formed in the test solution was recovered by vacuum filtration, where the filter holder was fitted with PTFE un-laminated membrane filters (0.45-micron, 47 mm from Sterlitech). All batch experiments were performed at room temperature.

### 2.3. Corrosion studies

The electrochemical corrosion studies were performed in various concentrations of the test solution (0.0077 M – 0.3 M) by using a homemade three-electrode cell system designed for flat electrodes connected to the potentiostat/galvanostat G3000-30111 (Gamry Instruments Inc., USA). The potentiodynamic polarization (PDP) curves were obtained by sweeping the electrode potential from -2.0 to +0.5 V versus open circuit potential at 0.5 mV $s^{-1}$ scan rate. The EC-Lab Version 10.1x Software package was used for data analysis and fitting. Gravimetric analysis was performed by placing the pure-Mg and the AZ31 alloy plates in various concentrations of the test solution (0.0077 M – 0.3 M) for 6 h. Before the tests, the plates were weighed. After 6 h, the plates were dried at room temperature and weighed again the following day, to calculate the mass loss.

### 2.4. Surface characterization

The elemental composition and morphology of the electrochemically produced struvite were evaluated by using a scanning electron microscope (SEM) (FEI Nova Nanolab 200 Dual-Beam). The electrochemically obtained struvite crystal sizes were determined from the SEM images by using NIH Image/ ImageJ, an open source image processing program. A PerkinElmer Frontier Fourier-transform infrared spectrometer (FT-IR) was used to characterize the chemical differences between commercially available struvite and struvite developed through experimental electrochemical

115 methods. FT-IR spectrophotometric analysis was carried out using infrared light with ten wavelength
116 scans from 4000 $cm^{-1}$ – 650 $cm^{-1}$ at a resolution of 4 $cm^{-1}$. The crystal structure analysis was
117 performed via x-ray diffraction (XRD) on a Philips PW1830 double system diffractometer equipped
118 with a Cu cathode.

119 **2.5. Calculations**

120 The expected magnesium release from the anode based on the measured current ($m_{Mg,current}$) was
121 evaluated according to Faraday's law of electrolysis using the following equation:

122 $$m_{Mg,\text{current}} = \frac{M_{Mg} Q}{zF} \quad (2)$$

123 where $z$ is the magnesium valence (2), $F$ is the Faraday constant (96485 C $mol^{-1}$), $M_{Mg}$ is the molar
124 mass of Mg (24.3 g $mol^{-1}$), and $Q$ is the electric charge (C) obtained from the integration of the $I$ vs.
125 $t$ curve (where $I$ is current in A and $t$ is time in s).

126 The dissolution rate of the Mg during the batch experiments was determined according to the
127 following equation:

128 $$v_{Mg} = \frac{m_{Mg,current}}{(t \text{ x } A)} \quad (3)$$

129 where $v_{Mg}$ is the rate of the total magnesium dissolved in the test solution (mg $cm^{-2}$ $h^{-1}$), $m_{Mg,current}$ is
130 the mass of the Mg dissolved (mg), $t$ is the time (h), and $A$ is the active surface area of the specific
131 anode ($cm^2$).

132 The measured corrosion current, from which the corrosion rate can be estimated from a Tafel-plot,
133 was obtained by performing a linear least square fit of the Butler-Volmer (Erdey-Gruz-Volmer)
134 equation to the data. The corrosion rate was estimated according to the following equation:

135 $$v_{corr} = \frac{I_{corr} \text{ x } K \text{ x } EW}{\rho \text{ x } A} \quad (4)$$

136 where $v_{corr}$ is the corrosion rate in millimeter per year (mmpy or mm $y^{-1}$), $I_{corr}$ is the corrosion current
137 (mA), $K$ is a constant that defines the units of the corrosion rate, $EW$ is the equivalent weight (g
138 $equivalent^{-1}$), $\rho$ is density (g $cm^{-3}$), and $A$ is the sample area ($cm^2$).

139

## 3. Results and Discussion

### 3.1. Electrochemical struvite formation and characterization

In our previous batch experiments, where we investigated electrochemical struvite precipitation using a sacrificial Mg anode as the only source for Mg in an acidic environment with no pH adjustment, the obtained percent yields (calculated based on the known starting concentrations of ammonium and phosphate in the test solution) were low, 11±3% for the pure-Mg and 3.0±0.8% for the AZ31 alloy anode, respectively. In other words, the % yield is equal to actual yield of struvite (i.e., the measured mass of struvite recovered from the reactor) divided by the theoretical yield of struvite based on the known starting concentrations of ammonium and phosphate multiplied by 100. To increase the percent yields and to improve struvite production, the SV/A was increased by 1.9-fold, from 0.047 $cm^{-1}$ to 0.089 $cm^{-1}$. The results of the 6 h batch experiments with the increased SV/A and no pH adjustment are shown in Table 1.

Similar to our previous measurements, the pH of the bulk test solution increased from an initial pH of 4.5±0.01 to 6.3±0.06 during the 6 h testing period. The theoretical Mg release ($m_{Mg,current}$), calculated according to Faraday's law of electrolysis (Eq. 2), was 0.343±0.03 g for the pure-Mg anode and 0.115±0.01 g for the AZ31 alloy. The new reactor system with the increased SV/A with the pure-Mg anode produced a 6.4-fold higher amount of struvite compared to AZ31 alloy. The production of 3.2±0.2 g of struvite corresponds to a 38±2% yield for the pure-Mg, while the production 0.5±0.1 g corresponds to only a 5±0.5% yield for the AZ31 alloy, where the percent yield was determined as described in the previous paragraph.

**// Table 1 //**

The Mg dissolution rates calculated according to Eq. 3 were 1.4 mg $cm^{-2}$ $h^{-1}$ for the pure-Mg anode and 0.5 mg $cm^{-2}$ $h^{-1}$ for the AZ31 Mg alloy anode, respectively. The increase of the SV/A seemed to have a powerful effect on the percent yield of struvite obtained for the pure-Mg anode, where an increase of a 27% was observed. On the other hand, the increase of the SV/A did not have a significant effect on the AZ31 alloy performance toward struvite production, where only a 2% increase in the obtained percent yield was observed. This result suggests that the corrosion resistance of the AZ31 Mg alloy is significantly higher compared to the pure-Mg anode, and that the formation of the insulating layer during the batch experiments has a dramatic outcome on the corrosion rates, which in turn can have a negative influence on the struvite precipitation.[31]

Surface chemical composition analysis was carried out on the struvite obtained in the batch experiments. The FT-IR spectra showed typical vibrational excitation of the functional groups characteristic and previously reported for struvite,[32-34] see Figure 2. The four distinct bonding regions specific to struvite are metal-oxygen bonds, hydrogen-amine bonds, oxygen-phosphorous bonds, and oxygen-hydrogen bonds.[35] The broad, complex, asymmetric band between 2325-3245 $cm^{-1}$ can be attributed to the O-H and N-H stretching vibrations, where the broad band at ~2900 $cm^{-1}$ indicates the $v_1$ symmetric stretching vibration of N-H. The band at 2342 $cm^{-1}$ is associated with the H-O-H stretching vibrations, while the bands at 1687-1585 $cm^{-1}$ are attributed to the water H-O-H bending region. The sharp peak at 1432 $cm^{-1}$ is an original band for N-H bending, while the symmetric P-O stretching vibration is visible as a robust, sharp peak at ~980 $cm^{-1}$ for all samples. The multiple bands observed at 885-755 $cm^{-1}$ represent the wagging modes of vibration of water molecules.

**// Figure 2 //**

The crystal structure of the solids was further characterized by XRD, and the results are shown in Figure 3, where the XRD patterns of the electrochemically obtained precipitates were compared to the pure struvite standard (PDF card no. 01-077-2303) and to the commercially available struvite (Crystal Green) as well. The XRD patterns showed no differences in the peak position; moreover, no additional diffraction peaks were observed, which would indicate the presence of another (interfering) mineral.[36, 37]

**// Figure 3 //**

The struvite samples obtained with 6 h batch experiments in 0.077 M ammonium dihydrogen phosphate using the pure-Mg or the AZ31 alloy as the anode were studied and analyzed by SEM, and the results are shown in Figure 4. In both cases, the results showed a morphology suggestive of the formation of high-quality pure struvite, with a needle-shaped elongated structure and smooth, sharp edges (NB: the sharp, smooth edges is a strong indication that there are no cations present in the crystal structure other than the expected cations of $Mg^{2+}$ and $NH_4^+$).[16] In other words, there are no foreign cations present that are not part of the expected struvite composition of $MgNH_4PO_4*6H_2O$. The reactor with the pure-Mg anode produced electrochemically precipitated struvite with a particle size of ca. 73 µm in length and ca. 13 µm in width (Figure 4A). The reactor with the AZ31 alloy anode produced smaller size struvite crystals of ca. 44 µm in length and ca 8 µm in width (Figure 4B). The smaller crystal sizes formed on the AZ31 alloy during the electrochemical measurements

may suggest the formation of a more compact insulating layer, which in turn would have a more drastic effect on electrochemically driven overall struvite formation.

**// Figure 4 //**

In a single-cell electrochemical batch reactor, the overall struvite production process is quite complicated and involves multiple reactions all co-occurring at the electrode surface.[14] In simplified terms, however, the electrochemically produced struvite depends mainly on the molar ratio of $Mg^{2+}$:$NH_4^+$:$PO_4^{3-}$ available in the test solution. However, in our setup the ratio of $Mg^{2+}$ to $NH_4^+$:$PO_4^{3-}$ changes significantly during the experiments. The concentration of the $Mg^{2+}$ ions in the test solution at the start of the batch experiments is minimal, and over time, due to the formation of the insulating layer, becomes finite, making the availability of magnesium a limiting factor. In this context, a solid comprehension of the corrosion process at the sacrificial anode and how the formation of the insulating layer affects the availability of the $Mg^{2+}$ becomes important.

### 3.2. Anode pitting behavior

As part of the electrochemical struvite precipitation study, we used an optical microscope to understand the morphological impact of magnesium corrosion on the electrode surface and the differences in morphology observed for the pure magnesium versus the AZ31 alloy; images were taken post-mortem after the 6 h batch tests and after struvite removal from the surface. The corrosion-induced pitting effect on pure-Mg and AZ31 Mg alloy anodes is shown in Figure 5, where a different pitting pattern can be observed between the two anode compositions. The differences in pitting morphology and growth can be associated with the different distribution of the Mg atoms on the surfaces of the anodes. In the case of pure Mg, where only Mg atoms are present, the pits form in a more inhomogeneous pattern, where larger diameter, interconnected pits, and irregular pitting were observed (Figure 5B).

The incorporation of Al and Zn atoms into the composition of the AZ31 alloy changes the subsequent pit morphology of the surface, where the composites are susceptible to galvanic or bimetallic corrosion.[38] The impurities present in the alloy composition likely form secondary phases within the alloy structure, where the grain boundaries are known to act as cathodes,[19, 24, 39, 40] compared to the body of the primary grains which are anodic and result in Mg corrosion. This difference in typical alloy grain morphology[41-44] also explains the small, more uniform pitting observed (Figure 5D) on the surface of the AZ31 alloy after the batch experiments, where the pitting is likely concentrated and localized at the sites where Mg atoms were present. Based on the uniform pitting throughout the

anode, it appears that the alloy composition has a homogeneous surface distribution of the Mg, Al, and Zn atoms.

**// Figure 5 //**

### 3.3. The effect of $NH_4H_2PO_4$ concentration on anode corrosion

To better understand the level of influence of the anode corrosion on the overall production of struvite in the electrochemical cell, PDP experiments were performed. The PDP curves recorded (not *i*R corrected) with the pure-Mg and the AZ31 alloy in various concentrations of dihydrogen ammonium phosphate are shown in Figure 6. From the curves, it can be observed that for all concentrations, there is a well-developed anodic branch in which the current density increases with potential; this behavior is consistent for both types of electrodes (pure-Mg shown in black and AZ31 alloy shown in red, Figure 6).

It is evident that during anodic polarization, the electrodes display similar behavior, whereas at the cathodic branch, the AZ31 alloy sustains significantly higher currents. At high anodic polarization, the anodic branch starts to deviate from Tafel behavior, while the formation of a passivating layer can be observed, which indicates the difficulty of $Mg^{2+}$ corrosive dissolution through this layer. The serration detected at this region is a clear evidence of a pitting corrosion mechanism. As expected, the number of serrations on the anodic branch increased with the salt concentration, which indicates higher corrosion rates.

**// Figure 6 //**

Different corrosion parameters such as the corrosion potential ($E_{corr}$), the corrosion current density ($j_{corr}$), the anodic ($\beta_a$) or the cathodic ($\beta_c$) Tafel constants, and the corrosion rate ($v_{corr}$) can be derived by Tafel extrapolation and are given in Table 2. As expected, the results show an increase in the corrosion current and corrosion rate with the increase of the salt concentration in the test solution for pure-Mg and the AZ31 alloy. This increase, however, produced an increase in the measured corrosion potential only for the AZ31 alloy, while in the case of pure-Mg anode, the corrosion potential did not change significantly. The calculated cathodic and anodic slopes show a direct correlation with electrolyte concentration for both anode types, where the slope generally increases with concentration, except for the highest electrolyte concentration and the pure-Mg anode. Under this condition, the Tafel slope drops to 146 mV, which is less than that calculated at 0.0077 M (168 mV). Shifts in Tafel slope value can indicate changes to reaction mechanism and changes in the rate-limiting step of the overall reaction, as well as overall reaction kinetics. A general increase in the

Tafel slope with concentration may suggest more sluggish kinetics, while a drop in the Tafel slope, such as that at 0.3 M for pure-Mg, could indicate changes at the electrode surface that enable increased reaction rate.

**// Table 2 //**

The obtained $j_{corr}$ for pure-Mg anode was 2-fold lower compared to the AZ31 alloy and this tendency increased with increasing salt concentration: 1.1-fold lower in 0.077 M, 4.3-fold lower in 0.15 M and 6.8-fold lower in 0.3 M ammonium dihydrogen phosphate, respectively (Table 2). Based on the corrosion rates obtained, the pure-Mg anode displayed a higher corrosion resistance compared to the AZ31 alloy in all the different salt concentrations tested. These results somewhat contradict the results obtained with the batch experiments, where the Mg dissolution rates were 2.8-fold higher when pure-Mg was used as the anode. However, we note that the corrosion potential, $E_{corr}$, for pure-Mg is more negative, indicating that this anode has a greater tendency to form metal ions and corrode than the AZ31 alloy.

The discrepancy in results between the PDP study (see Figure 6) and the single cell batch experiments, where Mg dissolution and struvite formation were measured, are also likely due to the difference in the electrochemical environment as a result of using a dynamic potential versus a constant potential experimental approach. In the single cell batch experiments, both anodes were held at -0.8 V vs. Ag/AgCl, which is a voltage well above the corrosion potentials measured for either anode. At this voltage, we expect the applied potential to drive the electrochemical magnesium corrosion even with struvite deposition on the surface of the electrodes, and for both electrodes, the measured current decreases to a non-zero, steady-state value. The PDP experiments (Figure 6), however, sweep across a range of voltage and likely cause dynamic behavior at the surface of the electrodes with regard to struvite formation. While PDP experiments are a traditional, well-known approach to evaluate the corrosion behavior of electrodes, these discrepancies suggest to us that this approach is non-ideal for the evaluation of Mg-based anodes in aqueous wastewater systems, where the complexity of the water chemistry and the deposition of particle layers on the surface of the electrode will confound the results and the information that can be garnered.

The discrepancy between the corrosion rates obtained by Tafel extrapolation from polarization curves and the Mg dissolution rates obtained from control-potential electrolysis, prompted us to investigate this matter further. The spontaneous (i.e., not driven by an applied voltage) corrosion of the sacrificial anodes was studied by weight loss analysis, where a set of experiments was performed for the salt

concentration range of 0.0077 M – 0.3 M. Surprisingly, instead of a weight loss, a weight gain was observed on the plates due to the deposition of a white precipitate. The precipitate was later analyzed by FT-IR and was found to be high quality pure struvite (results not shown). The relationship between the corrosion rates obtained from the PDP experiments and the measured mass of struvite deposited on the anode is presented graphically in Figure 7A,B.

In the case of pure-Mg (Figure 7A, filled circles), the corrosion rates increased linearly with the increase in the concentration of the test solution. The linear behavior of the corrosion rates indicated that the corrosion kinetics for the pure-Mg was independent of the growth of corrosion output/struvite on the surface. In the case of the AZ31 alloy (Figure 7A, empty circles), the corrosion rates showed an exponential increase with the increase of the salt concentration, which could suggest that mechanisms other than the salt concentration that surrounds the electrode are impacting the corrosion rate of the electrode. The mass of the insulating layer decreased exponentially with salt concentration for both types of anodes, see Figure 7B. It can be observed that the change in the corrosion rates versus the formation of the insulating layer of struvite on both pure-Mg and the AZ31 alloy has an inverse trend, supporting the conclusion that greater mass deposition of struvite on the anode surface has a direct impact on the decrease in corrosion rate.

// **Figure 7** //

Based on the gravimetric experiments, the amount of deposited struvite on the AZ31 alloy was higher compared to the pure-Mg in all salt concentrations: 1.7-fold (0.0077 M), 5.1-fold (0.077 M), 12.3-fold (0.15 M), and 5.5-fold (0.3 M), see Figure 7B. It seems that the struvite layer formation has a greater affinity towards the AZ31 alloy, which can be explained by the surface morphology of the alloy. Impurities such as Al present in the alloy composition changes the grain size, by forming the $\beta$-phase ($Mg_{17}Al_{12}$).[38] The presence of the $\beta$-phase increases the corrosion resistance of the alloy and shows a good passive behavior in broad pH ranges.[38] Previous studies performed by Song et al.[45, 46] showed that small grain size increased the corrosion resistance, while at the same time, the presence of large grain size decreased the corrosion resistance of the Mg alloy due to galvanic corrosion. These results (i.e., PDP and gravimetric measurements) remain in conflict with our single cell batch experiments, where applied voltage (-0.8 V) drives Mg corrosion and struvite formation, with pure-Mg outperforming AZ31 alloy in terms of struvite recovery, and therefore, $Mg^{2+}$ availability through electrode corrosion. We currently understand this conflicting result as potentially stemming from differences in electrode behavior under the chronoamperometric condition, as described above.

However, the gravimetric results may point to another aspect that would impact $Mg^{2+}$ release from the electrode surface: pure-Mg anodes have less struvite particles attached to the surface and thus, in a chronoamperometric environment, are able to corrode Mg at higher rates than the AZ31 alloy, which has either a more dense or thicker struvite layer on the surface (for the same tested electrode surface area).

The discrepancy between the corrosion potential, the corrosion current density and rates from the PDP results can thus be explained also by the formation of a passivating layer on the anode surface, which was observed and reported by others as well.[20, 47] It is obvious that during the 6 h batch and PDP experiments, the insulating film on the anodes decreases the ability of the dissolved $Mg^{2+}$ to diffuse into the solution and has an adverse effect on the corrosion rates, which in turn influences the formation of struvite. Based on Figure 7, we expect to be able to obtain significantly higher yields in high concentrations of the test solution. Since the level of phosphorus in wastewater is typically between 0.5-199 mg $L^{-1}$ ($1.6*10^{-5}$ – $6.4*10^{-3}$ M),[48, 49] the implication of this result is that the typical concentration of phosphorus (and ammonium) in wastewaters may need to be increased (e.g., concentrated through another process step) to increase the efficiency of the electrochemical struvite formation process. Further work in understanding how the efficiency of the electrochemical struvite precipitation process is impacted by salt concentration under chronoamperometric conditions is needed and will be included in our future work.

## Conclusions

In this work we demonstrated that the percent yield of the electrochemical struvite precipitation was significantly increased with the increase of the SV/A by 1.9-fold; however, it was only useful for the pure-Mg anodes, where a 27% increase was observed. For the AZ31 alloy, the increase of the SV/A did not produce a significant change in the percent yield. Based on the FT-IR and SEM analysis, a high-quality pure struvite was obtained, with the characteristic needle-shaped elongated structure and smooth, sharp edges. Potentiodynamic polarization experiments were performed to study the corrosion potential, rate and Tafel kinetics of the magnesium-based anodes. The results showed higher corrosion rates for the AZ31 alloy compared to the pure-Mg anode, which is in contradiction with the results obtained in the electrochemical batch experiments, where 2.8-fold higher magnesium dissolution rates were calculated for the pure-Mg anode. This discrepancy between the techniques was attributed to the difference in the electrochemical environment as a result of changing potential

versus constant potential experimental approach, and the formation of the insulating layer on the anodes during the batch experiments. It seems that the insulating layer formed on the AZ31 alloy during the batch experiments have a more significant influence on the corrosion rates which in turn have an unfavorable effect on the overall struvite production.

## Acknowledgments

LKN, FA, and LFG acknowledge the National Science Foundation (NSF) for financial support of this work through the INFEWS/T3 Award# 1739473. The team thanks Ostara Nutrient Recovery Technologies, Inc. for generously providing samples of Crystal Green product for experiments and testing.

**Partial Support** – We acknowledge partial support from the Center for Advanced Surface Engineering, under the National Science Foundation Grant No. IIA-1457888 and the Arkansas EPSCoR Program, ASSET III.

**Equipment/Facilities** – Funding (or partial funding) for equipment/facilities used in this research was provided by the Center for Advanced Surface Engineering, under the National Science Foundation Grant No. IIA-1457888 and the Arkansas EPSCoR Program, ASSET III.

## References

1. L. E. De-Bashan and Y. Bashan, *Water Res,* **38** (19), 4222-4246 (2004).
2. Y. Jaffer, T. A. Clark, P. Pearce, and S. A. Parsons, *Water Res,* **36** (7), 1834-1842 (2002).
3. K. S. Le Corre, E. Valsami-Jones, P. Hobbs, and S. A. Parsons, *Crit. Rev. Environ. Sci. Technol.,* **39** (6), 433-477 (2009).
4. B. Li, I. Boiarkina, W. Yu, H. M. Huang, T. Munir, G. Q. Wang, and B. R. Young, *Sci. Total. Environ.,* (2018).
5. H. Li, S.-H. Yu, Q.-Z. Yao, G.-T. Zhou, and S.-Q. Fu, *RSC Adv.,* **5** (111), 91601-91608 (2015).
6. J. D. Doyle, K. Oldring, J. Churchley, and S. A. Parsons, *Water Res,* **36** (16), 3971-3978 (2002).
7. R. D. Cusick and B. E. Logan, *Bioresour. Technol.,* **107** 110-115 (2012).
8. M. S. Massey, J. G. Davis, J. A. Ippolito, and R. E. Sheffield, *Agron. J.,* **101** (2), 323-329 (2009).
9. C.-C. Wang, X.-D. Hao, G.-S. Guo, and M. C. M. Van Loosdrecht, *Chem. Eng. J.,* **159** (1-3), 280-283 (2010).
10. B. Tansel, G. Lunn, and O. Monje, *Chemosphere,* **194** 504-514 (2018).
11. D. J. Kruk, M. Elektorowicz, and J. A. Oleszkiewicz, *Chemosphere,* **101** 28-33 (2014).
12. N. C. Bouropoulos and P. G. Koutsoukos, *J. Cryst. Growth.,* **213** (3-4), 381-388 (2000).
13. S. Ben Moussa, G. Maurin, C. Gabrielli, and M. B. Amor, *Electrochem. Solid State Lett.,* **9** (6), C97-C101 (2006).
14. A. Hug and K. M. Udert, *Water Res,* **47** (1), 289-299 (2013).

15. Z. Belarbi and J. P. Trembly, *J. Electrochem. Soc. ,* **165** (13), E685-E693 (2018).
16. K. S. Le Corre, E. Valsami-Jones, P. Hobbs, and S. A. Parsons, *J. Cryst. Growth,* **283** (3-4), 514-522 (2005).
17. M. P. Huchzermeier and W. Tao, *Water Environ. Res.,* **84** (1), 34-41 (2012).
18. C. Kappel, K. Yasadi, H. Temmink, S. J. Metz, A. J. B. Kemperman, K. Nijmeijer, A. Zwijnenburg, G.-J. Witkamp, and H. H. M. Rijnaarts, *Sep. Purif. Technol.,* **120** 437-444 (2013).
19. M. Esmaily, J. E. Svensson, S. Fajardo, N. Birbilis, G. S. Frankel, S. Virtanen, R. Arrabal, S. Thomas, and L. G. Johansson, *Prog. Mater. Sci.,* **89** 92-193 (2017).
20. G. Song and A. Atrens, *Adv. Eng. Mater.,* **5** (12), 837-858 (2003).
21. O. Lunder, J. E. Lein, T. K. Aune, and K. Nisancioglu, *Corrosion,* **45** (9), 741-748 (1989).
22. R.-c. Zeng, J. Zhang, W.-j. Huang, W. Dietzel, K. U. Kainer, C. Blawert, and K. E. Wei, *Trans. Nonferrous Met. Soc. China,* **16** s763-s771 (2006).
23. F. W. Richey, B. D. McCloskey, and A. C. Luntz, *J. Electrochem. Soc.,* **163** (6), A958-A963 (2016).
24. G. L. Song and A. Atrens, *Adv. Eng. Mater.,* **1** (1), 11-33 (1999).
25. L. G. Bland, A. D. King, N. Birbilis, and J. R. Scully, *Corrosion,* **71** (2), 128-145 (2014).
26. A. Atrens, G.-L. Song, F. Cao, Z. Shi, and P. K. Bowen, *J. Alloys. Compd.,* **1** (3), 177-200 (2013).
27. A. Pardo, S. Feliu, M. C. Merino, R. Arrabal, and E. Matykina, *Int. J. Corros. ,* **2010** (2010).
28. M. E. Straumanis and B. K. Bhatia, *J. Electrochem. Soc.,* **110** (5), 357-360 (1963).
29. G. S. Frankel, A. Samaniego, and N. Birbilis, *Corros. Sci.,* **70** 104-111 (2013).
30. M. Stern and A. L. Geary, *J. Electrochem. Soc.,* **104** (1), 56-63 (1957).
31. N. Hutnik, A. Kozik, A. Mazienczuk, K. Piotrowski, B. Wierzbowska, and A. Matynia, *Water Res,* **47** (11), 3635-3643 (2013).
32. V. Stefov, B. Šoptrajanov, F. Spirovski, I. Kuzmanovski, H. D. Lutz, and B. Engelen, *J. Mol. Struct.,* **689** (1-2), 1-10 (2004).
33. V. Stefov, B. Šoptrajanov, I. Kuzmanovski, H. D. Lutz, and B. Engelen, *J. Mol. Struct.,* **752** (1-3), 60-67 (2005).
34. Z.-L. Ye, S.-H. Chen, M. Lu, J.-W. Shi, L.-F. Lin, and S.-M. Wang, *Wat. Sci. Tech.,* **64** (2), 334-340 (2011).
35. T. Zhang, P. Li, C. Fang, and R. Jiang, *Ecol. Chem. Eng. S.,* **21** (1), 89-99 (2014).
36. M. I. H. Bhuiyan, D. S. Mavinic, and F. A. Koch, *Chemosphere,* **70** (8), 1347-1356 (2008).
37. K. Z. Chong and T. S. Shih, *Mater. Chem. Phys.,* **80** (1), 191-200 (2003).
38. I. B. Singh, M. Singh, and S. Das, *Journal of Magnesium and Alloys,* **3** (2), 142-148 (2015).
39. A. Pardo, S. Feliu, M. C. Merino, R. Arrabal, and E. Matykina, *International Journal of Corrosion,* **2010** (2010).
40. P. Lin, K. T. Aust, G. Palumbo, and U. Erb, *Scr. Mater.,* **33** (9), (1995).
41. U. F. H. R. Suhuddin, S. Mironov, Y. S. Sato, H. Kokawa, and C.-W. Lee, *Acta Mater.,* **57** (18), 5406-5418 (2009).
42. A. K. Dahle, Y. C. Lee, M. D. Nave, P. L. Schaffer, and D. H. StJohn, *J. LIGHT MET,* **1** (1), 61-72 (2001).
43. N. N. Aung and W. Zhou, *Corr. Sci.,* **52** (2), 589-594 (2010).
44. S. M. Yin, F. Yang, X. M. Yang, S. D. Wu, S. X. Li, and G. Y. Li, *Mater. Sci. Eng., A,* **494** (1-2), 397-400 (2008).
45. G. Song, A. Atrens, and M. Dargusch, *Corr. Sci.,* **41** (2), 249-273 (1998).
46. G. Song, A. Atrens, X. Wu, and B. Zhang, *Corr. Sci.,* **40** (10), 1769-1791 (1998).
47. X. Lin, Z. Han, H. Yu, Z. Ye, S. Zhu, and J. Zhu, *J. Clean. Prod.,* **174** 1598-1607 (2018).
48. S. Aslan and I. K. Kapdan, *Ecol. Eng.,* **28** (1), 64-70 (2006).
49. L. Xin, H. Hong-ying, G. Ke, and S. Ying-xue, *Bioresour. Technol.,* **101** (14), 5494-5500 (2010).

Table 1. Initial and final pH of the test solution, theoretical Mg release, the actual Mg release, current density, the amount of struvite and the yields obtained with the different anodes.

| Anode | $pH_i$ [a] | $pH_f$ [b] | $m_{Mg,current}$ [c] (g) | $m_{struvite}$ [d] (g) | Yield[e] (%) |
|---|---|---|---|---|---|
| Pure-Mg | 4.5±0.01 | 6.3±0.06 | 0.343±0.03 | 3.2±0.2 | 38±2 |
| AZ31 | 4.4±0.03 | 5.9±0.06 | 0.115±0.01 | 0.5±0.1 | 5±0.5 |

[a]initial bulk pH; [b]final bulk pH; [c]theoretical Mg release according to Eq. 3; [d]amount of struvite obtained after 6 h batch experiments and [e]percent yield obtained from the known initial amount of ammonium and phosphate in the test solution.

Table 2. The different corrosion parameters obtained for Mg and AZ31 alloy anodes derived from the Tafel plots in different concentrations of synthetic wastewater.

| Anode | $[NH_4H_2PO_4]$ (M) | $E_{corr}$ vs Ag/AgCl (V) | $j_{corr}$ (mA $cm^{-1}$) | $\beta_c$ (mV) | $\beta_a$ (mV) | $v_{corr}$ [a] (mm $y^{-1}$) |
|---|---|---|---|---|---|---|
| Pure Mg | 0.0077 | -1.89 | 0.02 | 210 | 168 | 0.24 |
| | 0.077 | -1.82 | 0.07 | 422 | 339 | 1.01 |
| | 0.15 | -1.82 | 0.08 | 462 | 253 | 1.18 |
| | 0.3 | -1.84 | 0.13 | 519 | 146 | 2.08 |
| AZ31 alloy | 0.0077 | -1.74 | 0.04 | 378 | 363 | 0.65 |
| | 0.077 | -1.62 | 0.08 | 324 | 306 | 1.25 |
| | 0.15 | -1.54 | 0.34 | 653 | 474 | 5.08 |
| | 0.3 | -1.47 | 0.88 | 635 | 455 | 13.22 |

[a]the corrosion rate in millimeter per year according to Eq. 4

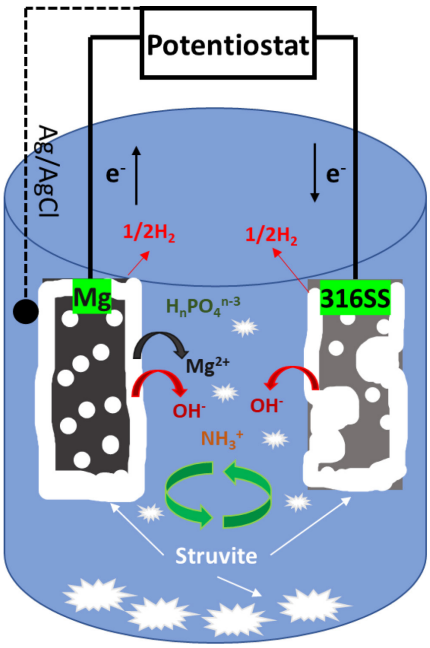

**Figure 1.** The schematic illustration of the electrochemical setup used for the precipitation of struvite, where the magnesium anode was the only source for magnesium and used as a sacrificial anode. In the course of the experiments, $Mg^{2+}$ (due to corrosion), $H_2$ and $OH^-$ are formed on the anode surface, while on the cathode $H_2O$ is reduced to $H_2$ and $OH^-$, where the latter will increase the local pH.

451

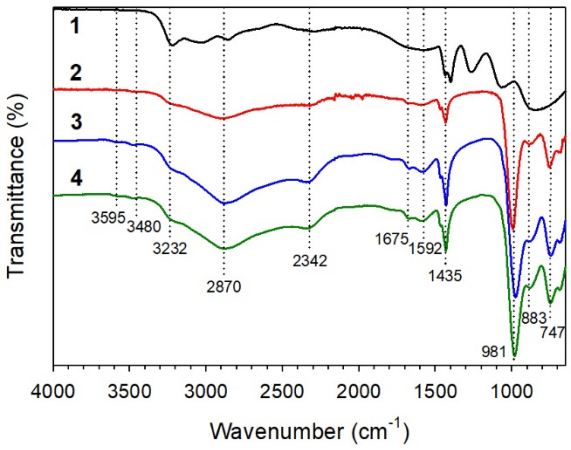


**Figure 2.** The FTIR spectra of (1) ammonium dihydrogen phosphate; (2) commercially available struvite (Crystal Green); struvite formed electrochemically with (3) pure-Mg; and (4) AZ31 Mg alloy in 0.077 M ammonium dihydrogen phosphate after 6 h batch experiment.

452

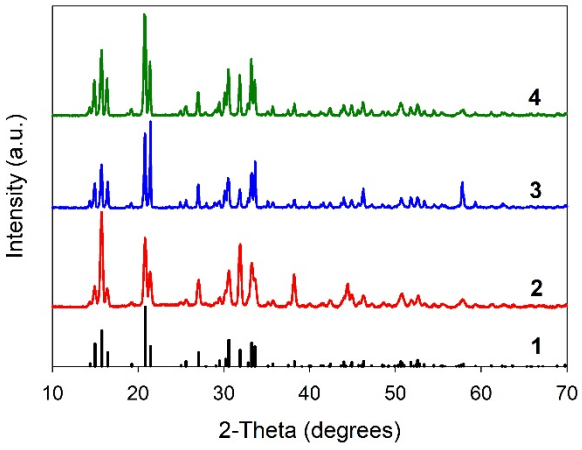


**Figure 3.** The XRD patterns of the (1) struvite standard (PDF card no. 01-077-2303); (2) commercially available struvite (Crystal Green); and struvite formed electrochemically with (3) pure-Mg; (4) AZ31 Mg alloy used as anode.

453

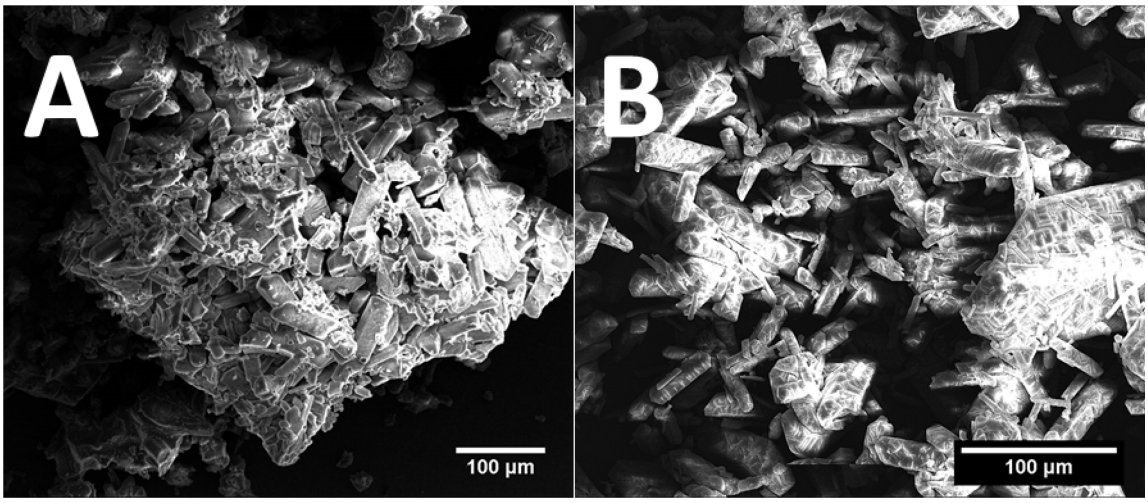


**Figure 4.** SEM images of the obtained struvite after 6-hour batch experiments in 0.0077 M test solution, in reactors where (A) pure-Mg and (B) AZ31 alloy were used as anodes.

454

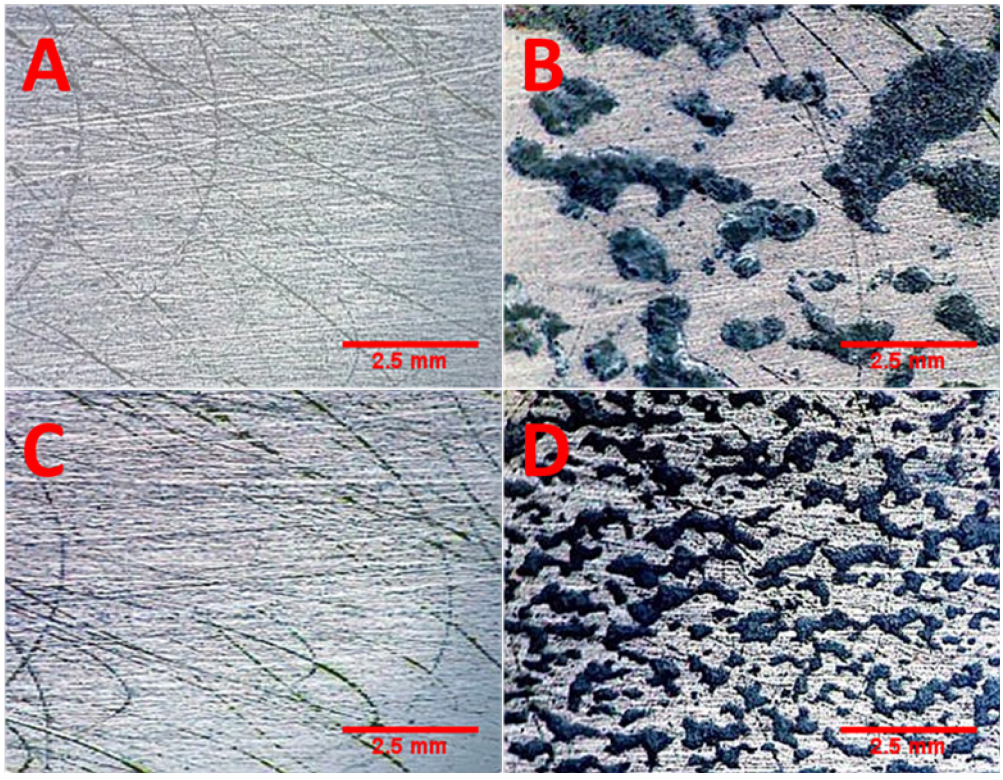


**Figure 5.** Optical images obtained of the surface of the Mg anode (top) (A) before and (B) after a 6 h batch experiment in 0.077 M ammonium dihydrogen phosphate. Optical images of the surface of the AZ31 alloy (bottom) (C) before and (D) after a 6 h batch experiment in 0.077 M ammonium dihydrogen phosphate.

455

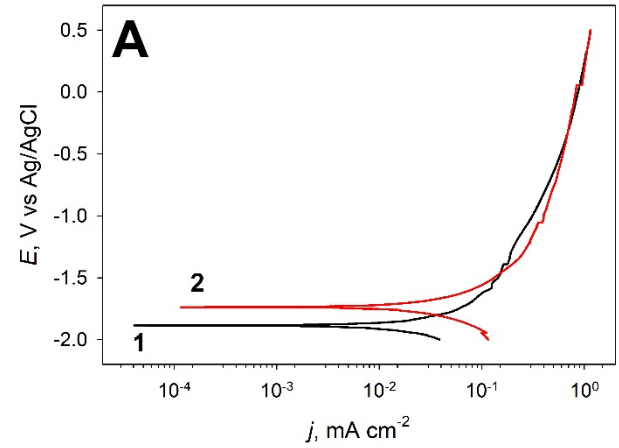
A
0.5
0.0
-0.5
-1.0
-1.5
-2.0
E, V vs Ag/AgCl
2
1
10-4
10-3
10-2
10-1
100
j, mA cm-2

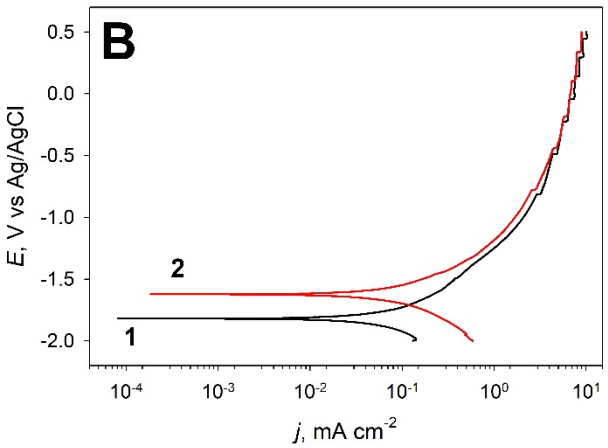
B
0.5
0.0
-0.5
-1.0
-1.5
-2.0
E, V vs Ag/AgCl
2
1
10-4
10-3
10-2
10-1
100
101
j, mA cm-2

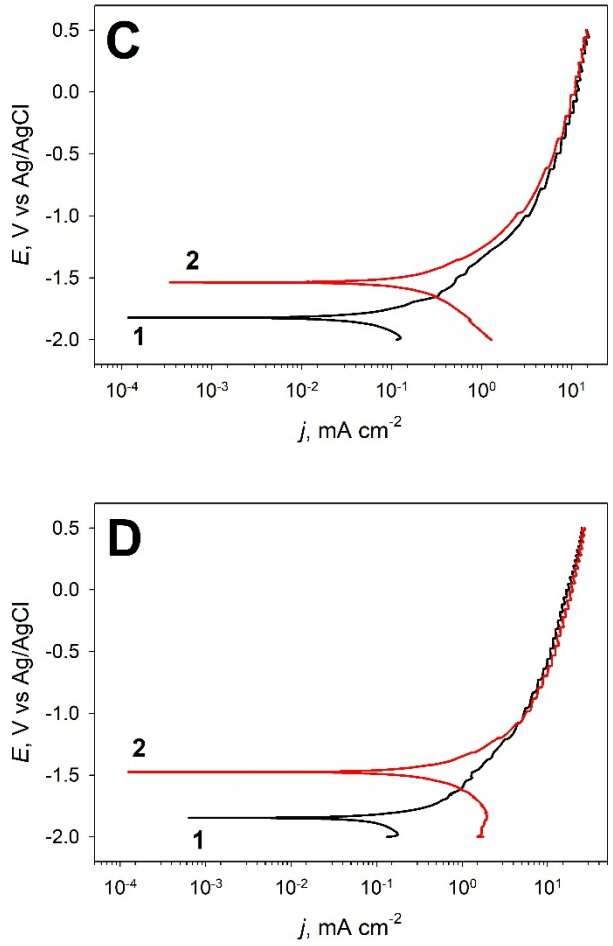


**Figure 6.** Potentiodynamic polarization curves obtained in (A) 0.0077 M, (B) 0.077 M, (C) 0.15 M, and (C) 0.3 M dihydrogen ammonium phosphate using (1) pure-Mg and (2) AZ31 magnesium alloy as anode, at room temperature.

456

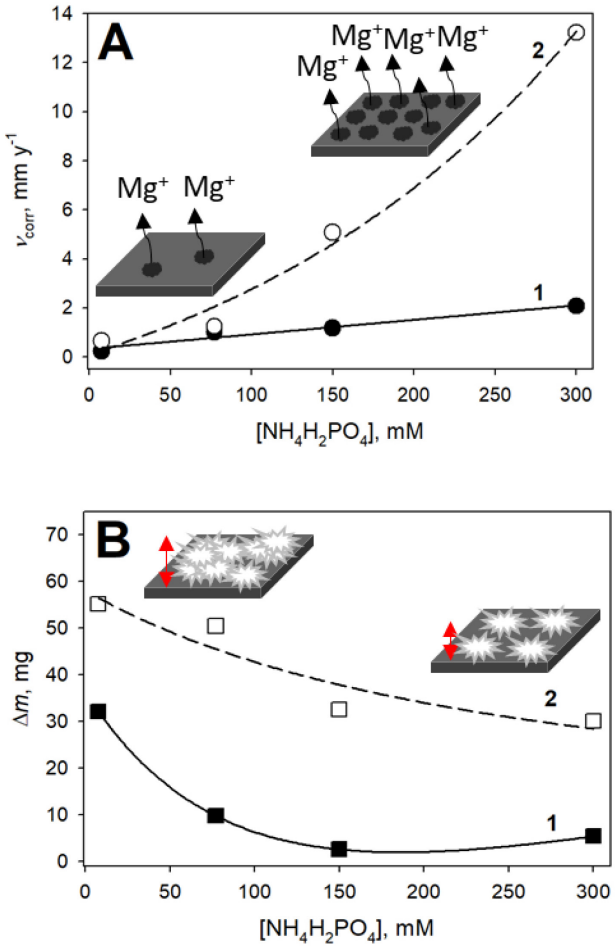


**Figure 7.** (A) The corrosion rates derived from the Tafel slopes in the PDP experiments and (B) the mass of struvite deposited during the gravimetric experiments on the (1) pure-Mg and (2) AZ31 alloy anodes, placed in various concentrations of dihydrogen ammonium phosphate: 0.0077, 0.077, 0.15 and 0.3 M, respectively. Gravimetric experiments were performed without an applied voltage or a connected electric circuit.

457